Supplementary materials for

ATF2 drives macrophage-mediated anti-PD-1 resistance by coupling KAT3A-dependent H3K18 lactylation with CCL2 transcription in hepatocellular carcinoma

Conghuan Shen[1,#], Yuchen Hou[2,3,4,#], Changjie Yang[5,#], Fangqi Ma[6,#], Ensi Ma[1,2], Hongyuan Xue[1,2], Chao Sun[1,2], Li Li[1,2], Jianhua Li[1,2], Ruipeng Song[2,3,4,*],Qing Wang[7], Jizhou Wang[2,3,4,*], Zhengxin Wang[1,*, §]

Affiliation:

1. Liver Transplantation Center, Department of General Surgery, Huashan Hospital & Institute of Organ Transplantation, Fudan University, Shanghai 200040, China.

2. Department of Hepatobiliary Surgery, the First Affiliated Hospital of USTC, Division of Life Sciences and Medicine, University of Science and Technology of China, Hefei, Anhui, 230001, P.R. China.

3. Anhui Province Key Laboratory of Hepatopancreatobiliary Surgery, Hefei, Anhui, P.R. China.

4. Anhui Provincial Clinical Research Center for Hepatobiliary Diseases, Hefei, Anhui, P.R. China.

5. Department of Gastrointestinal Surgery, Renji Hospital, Shanghai Jiao Tong University School of Medicine, Shanghai, 200120, P.R. China

6. Department of Hepatobiliary Surgery, the First Affiliated Hospital of USTC, Division of Life Sciences and Medicine, University of Science and Technology of China, Hefei, Anhui, 230001, P.R. China.

7. Department of Medical Oncology, Zhongshan Hospital, Fudan University, Shanghai, 200032, P.R. China.

[#] These authors contribute equally to this work.

§ Lead contact

***Correspondence to:**

Zhengxin Wang (wangzhengxin@huashan.org.cn), Liver Transplantation Center, Department of General Surgery, Huashan Hospital & Institute of Organ Transplantation, Fudan University, Shanghai 200040, China.

Jizhou Wang (wangjoe@ustc.edu.cn), Department of Hepatobiliary Surgery, the First Affiliated Hospital of USTC, Division of Life Sciences and Medicine, University of Science and Technology of China, Hefei, Anhui, 230001, P.R. China.

Qing Wang (wang.qing2@zs-hospital.sh.cn), Department of Medical Oncology, Zhongshan Hospital, Fudan University, Shanghai, 200032, P.R. China.

Ruipeng Song (songruipeng@ustc.edu.cn), Department of Hepatobiliary Surgery, the First Affiliated Hospital of USTC, Division of Life Sciences and Medicine, University of Science and Technology of China, Hefei, Anhui, 230001, P.R. China.

Supplementary methods

Vectors and transfections

Lentiviral vectors were used for stable gene knockout, knockdown, overexpression, and rescue experiments in HCC cells. For ATF2 knockout in murine TIBx cells, single-guide RNAs targeting mouse Atf2 were cloned into the lentiCRISPR v2 vector (Addgene, Cat# 52961). For stable knockdown of human ATF2, CCL2, and RELA/p65, short hairpin RNA sequences were cloned into the pLKO.1-puro vector (Addgene, Cat# 8453). For ATF2 or CCL2 overexpression and rescue experiments, full-length human ATF2 or CCL2 coding sequences were cloned into the pLVX-Puro lentiviral expression vector (Takara Bio, Cat# 632164). Empty lentiCRISPR v2, pLKO.1-puro, or pLVX-Puro vectors were used as corresponding negative controls. All sgRNA, shRNA, and cloning primer sequences are listed in Supplementary Table S2. All plasmids were confirmed by Sanger sequencing before use.

Lentiviral particles were produced in HEK293T cells by co-transfecting the transfer plasmid with the packaging plasmid psPAX2 (Addgene, Cat# 12260) and the envelope plasmid pMD2.G (Addgene, Cat# 12259) using Lipofectamine 3000 Transfection Reagent (Invitrogen, Cat# L3000015). HEK293T cells were maintained in DMEM (Gibco, Cat# 11965092) supplemented with 10% fetal bovine serum (Gibco, Cat# 10099141C) and 1% penicillin-streptomycin solution (Gibco, Cat# 15140122). Viral supernatants were collected at 48 h and 72 h after transfection, centrifuged at 500 × g for 10 min to remove cell debris, and filtered through 0.45 μm PVDF filters (Millipore, Cat# SLHV033RB).

For lentiviral transduction, target cells were seeded one day before infection and incubated with viral supernatants supplemented with 8 μg/mL polybrene (Sigma-Aldrich, Cat# H9268). After 24 h, the medium was replaced with fresh complete medium. Stable cells were selected with puromycin dihydrochloride (InvivoGen, Cat# ant-pr-1) at 2 μg/mL for human HCC cell lines and 4 μg/mL for murine HCC cell lines for 5-7 days. Knockout, knockdown, or overexpression

efficiency was verified by RT-qPCR and Western blotting before functional experiments.

For in vivo experiments, ATF2-knockout TIBx cells and control TIBx cells were used to establish ATF2 loss-of-function orthotopic liver tumor models. ATF2-overexpressing Hepa 53.4 cells and vector-control Hepa 53.4 cells were used to establish ATF2 gain-of-function orthotopic liver tumor models. For in vitro macrophage co-culture and migration assays, ATF2 was stably knocked down in ATF2-high HCC cells, including Huh-7 and SNU-387, whereas ATF2 was stably overexpressed in ATF2-low HCC cells, including SNU-475 and JHH-4. To determine whether CCL2 mediates the effect of ATF2 on macrophage recruitment and M2-like polarization, CCL2 was knocked down in ATF2-overexpressing SNU-475 and JHH-4 cells, and CCL2 expression was restored in ATF2-knockdown Huh-7 and SNU-387 cells.

For NF-κB pathway validation, RELA/p65 was stably knocked down in Huh-7 cells using pLKO.1-shRELA lentiviral vectors. For screening histone lactylation writer enzymes, small interfering RNAs targeting KAT3A/CREBBP, KAT3B/EP300, and other indicated KAT family members were transfected into HCC cells using Lipofectamine RNAiMAX Transfection Reagent (Invitrogen, Cat# 13778150) according to the manufacturer's instructions. A non-targeting siRNA was used as the negative control. Cells were harvested 48-72 h after siRNA transfection for RT-qPCR, Western blotting, ChIP-qPCR, or downstream functional analyses. The siRNA sequences are listed in Supplementary Table S2.

For plasmid transfection in luciferase reporter assays, Huh-7 cells were transfected with pGL3-CCL2 promoter reporter constructs and pRL-TK Renilla plasmid using Lipofectamine 3000 Transfection Reagent. Cells were harvested 48h after transfection for dual-luciferase activity measurement. For all genetic manipulation experiments, only cell populations with validated knockout, knockdown, or overexpression efficiency were used for subsequent assays.

GW2580 treatment

To pharmacologically inhibit macrophage accumulation and M2-like polarization, tumor-bearing mice were treated with the CSF1R inhibitor GW2580 (Selleck Chemicals, Cat# S8042). GW2580 was dissolved in DMSO and further diluted in vehicle solution consisting of 0.5% carboxymethylcellulose sodium (CMC-Na; Sigma-Aldrich, Cat# C4888) and 0.1% Tween-80 (Sigma-Aldrich, Cat# P4780). Mice received GW2580 at 160 mg/kg by oral gavage once daily, starting 5-7 days after tumor implantation and continuing until the experimental endpoint. Control mice received the same volume of vehicle. Tumor tissues were collected for flow cytometric analysis of $CD86^+$ M1-like and $CD206^+$ M2-like macrophages, $CD8^+$ T-cell infiltration, and T-cell functional markers.

ATF2 inhibitor and αPD-1 treatment

For therapeutic intervention experiments, orthotopic HCC-bearing mice were randomly assigned to the following groups: vehicle control, αPD-1 monotherapy, SBI-0087702 monotherapy, and SBI-0087702 plus αPD-1 combination therapy. The ATF2 inhibitor SBI-0087702 (MedChemExpress, Cat# HY-134963) was dissolved in DMSO and diluted in vehicle containing 10% DMSO, 40% PEG300 (MedChemExpress, Cat# HY-Y0873), 5% Tween-80, and 45% sterile saline. SBI-0087702 was administered intraperitoneally at 25 mg/kg every 3 days starting 7 days after tumor implantation.

For PD-1 blockade, mice were treated with anti-mouse PD-1 monoclonal antibody (Bio X Cell, clone RMP1-14, Cat# BE0146) at 10 mg/kg by intraperitoneal injection every 3 days. Control mice received the corresponding isotype control antibody, rat IgG2a (Bio X Cell, clone 2A3, Cat# BE0089), at the same dose and schedule. Combination-treated mice received both SBI-0087702 and anti-PD-1 antibody according to the schedules described above. Tumor burden was evaluated by tumor weight and gross tumor size at the endpoint. For survival experiments, treatment was

continued until mice reached predefined humane endpoints.

Tissue collection and immune profiling

At the indicated endpoints, mice were euthanized, and orthotopic liver tumors were carefully excised, weighed, photographed, and processed for downstream analyses. For flow cytometry, freshly isolated tumor tissues were processed as described in the Flow cytometry section. For histological and immunofluorescence analyses, tumor tissues and major organs were fixed in 4% paraformaldehyde, embedded in paraffin, sectioned, and subjected to H&E staining, immunohistochemistry, or immunofluorescence staining. For molecular assays, fresh tumor tissues were snap-frozen in liquid nitrogen and stored at -80°C until RNA or protein extraction.

Serum biochemistry and safety evaluation

To evaluate systemic toxicity, peripheral blood was collected from mice at the experimental endpoint using serum separator tubes (BD Microtainer, Cat# 365967). Serum was isolated by centrifugation at 3,000 × g for 10 min at 4°C and subjected to biochemical analysis. Serum alanine aminotransferase (ALT; Nanjing Jiancheng Bioengineering Institute, Cat# C009-2-1), aspartate aminotransferase (AST; Nanjing Jiancheng Bioengineering Institute, Cat# C010-2-1), albumin (ALB; Nanjing Jiancheng Bioengineering Institute, Cat# A028-2-1), urea nitrogen (UREA/BUN; Nanjing Jiancheng Bioengineering Institute, Cat# C013-2-1), creatinine (CREA; Nanjing Jiancheng Bioengineering Institute, Cat# C011-2-1), creatine kinase (CK; Nanjing Jiancheng Bioengineering Institute, Cat# A032-1-1), and glucose (GLU; Nanjing Jiancheng Bioengineering Institute, Cat# F006-1-1) levels were measured using commercial assay kits according to the manufacturer's instructions. Major organs, including heart, spleen, lung, brain, and kidney, were fixed in 4% paraformaldehyde solution (Beyotime, Cat# P0099), embedded in paraffin, sectioned, and stained using an H&E staining kit (Servicebio, Cat# G1005) to assess

histopathological toxicity.

Public dataset analysis

scRNA-seq datasets and processing. We collected publicly available single-cell RNA sequencing (scRNA-seq) datasets from three independent HCC cohorts (CRA002308, GSE149614, and GSE242889), encompassing a total of 44,683 cells from 38 human tumor or adjacent-normal (AN) samples. Data processing was performed using the Seurat (v4.3) R package. After data normalization, scaling, dimension reduction (PCA and UMAP), and batch-correction, we performed unsupervised clustering and annotated major myeloid subpopulations (macrophages, monocytes, dendritic cells, etc.) based on canonical marker expression (e.g., CD68, CD163, APOE for macrophages; ITGAX, CLEC9A for dendritic cells; FCN1 for monocytes; S100A8/S100A9 for neutrophils).

TCGA and GEO data analysis. HCC cohort datasets from The Cancer Genome Atlas (TCGA) (https://www.cancer.gov/ccg/research/genome-sequencing/tcga) and Gene Expression Omnibus (GEO) (https://www.ncbi.nlm.nih.gov/geo/) were analyzed to compare gene expression levels between tumor and adjacent normal tissues, and to assess gene correlations.

Spatial transcriptomic analysis. For a subset of patients treated with αPD-1 (responders vs. non-responders), spatial transcriptomic data (PMID: 36708811) were used to map the distribution of M2-macrophage markers (e.g., CD206, SPP1). Spatial cell-density quantification was performed using STUtility / Seurat pipelines to compare M2-macrophage infiltration in tumor regions between responsive and non-responsive cases.

Macrophage polarization analysis

Macrophage polarization was assessed by RT-qPCR and flow cytometry. For

RT-qPCR analysis, total RNA was extracted from THP-1-derived macrophages using TRIzol Reagent (Invitrogen, Cat# 15596026), and cDNA was synthesized using the PrimeScript RT reagent Kit with gDNA Eraser (Takara, Cat# RR047A). Quantitative PCR was performed using TB Green Premix Ex Taq II (Takara, Cat# RR820A) on a real-time PCR system according to the manufacturer's instructions. The expression of M1-associated genes, including NOS2, CXCL10, CXCL9, and TNF-α, and M2-associated genes, including CD206/MRC1, CD163, ARG1, TGF-β1, and IL-10, was analyzed. Relative gene expression was calculated using the $2^{-\Delta\Delta Ct}$ method and normalized to GAPDH.

For flow cytometric analysis, macrophages were harvested, washed twice with cold PBS, and resuspended in Cell Staining Buffer (BioLegend, Cat# 420201). Cells were incubated with Human TruStain FcX Fc receptor blocking solution (BioLegend, Cat# 422302) for 10 min at 4°C and then stained with Zombie NIR Fixable Viability Kit (BioLegend, Cat# 423105), PE-conjugated anti-human CD86 antibody (BioLegend, clone IT2.2, Cat# 305406), and APC-conjugated anti-human CD206 antibody (BioLegend, clone 15-2, Cat# 321110) for 30 min at 4°C in the dark. Corresponding fluorochrome-conjugated isotype controls were used where appropriate. After staining, cells were washed, resuspended in staining buffer, and analyzed using a BD LSRFortessa flow cytometer. Data were analyzed with FlowJo software.

Migration assays

Conditioned media were collected from HCC cells or HCC cell-macrophage co-culture systems after 48 h of culture. Cells were then washed twice with sterile PBS (Gibco, Cat# 10010023) and cultured in serum-free DMEM or RPMI 1640 medium for 48 h. The supernatants were collected, centrifuged at 1,000 × g for 10 min to remove cell debris, and filtered through a 0.22 μm filter before use.

Macrophage migration was assessed using 24-well Transwell chambers with 8.0 μm pore polycarbonate membrane inserts (Corning, Cat# 3422). PMA-differentiated

THP-1-derived macrophages were harvested, washed twice with PBS, and resuspended in serum-free RPMI 1640 medium. A total of 1 × 10^5 macrophages in 200 μL serum-free medium were seeded into the upper chamber, while 600 μL of HCC cell-derived CM was added to the lower chamber as the chemoattractant. Serum-free medium was used as the negative control where appropriate.

After incubation for 6 h at 37°C in a humidified incubator containing 5% CO_2, non-migrated cells on the upper surface of the membrane were gently removed with cotton swabs. Migrated cells attached to the lower surface of the membrane were fixed with 4% paraformaldehyde solution (Beyotime, Cat# P0099) for 15 min at room temperature and stained with crystal violet staining solution (Beyotime, Cat# C0121) for 15-20 min. Membranes were washed with PBS, air-dried, and imaged under a light microscope. Migrated cells were counted in at least five randomly selected fields per insert. Each experiment was performed in triplicate.

Co-immunoprecipitation and IP-re-IP assays

Co-immunoprecipitation (Co-IP) assays were performed to examine the interaction between ATF2 and KAT3A/CBP in HCC cells. Briefly, Huh-7 cells were harvested, washed twice with ice-cold PBS (Gibco, Cat# 10010023), and lysed in IP lysis buffer from the Pierce Crosslink Magnetic IP/Co-IP Kit (Thermo Fisher Scientific, Cat# 88805) supplemented with protease inhibitor cocktail (Roche, Cat# 11873580001) and phosphatase inhibitor cocktail (Roche, Cat# 4906845001). Cell lysates were incubated on ice for 30 min and centrifuged at 12,000 × g for 15 min at 4°C. Protein concentrations were determined using the Pierce BCA Protein Assay Kit (Thermo Fisher Scientific, Cat# 23225).

For endogenous Co-IP, equal amounts of protein lysates were pre-cleared with Pierce Protein A/G Magnetic Beads and then incubated overnight at 4°C with antibodies against ATF2 (Cell Signaling Technology, Cat# 35031), KAT3A/CBP/CREBBP (Abcam, Cat# ab2832), NF-κB p65/RELA (Cell Signaling Technology, Cat# 6956), normal

rabbit IgG (Cell Signaling Technology, Cat# 2729), or normal mouse IgG (Cell Signaling Technology, Cat# 5415). Antibody–protein complexes were captured using Pierce Protein A/G Magnetic Beads according to the manufacturer's instructions. After extensive washing with IP lysis/wash buffer, bound proteins were eluted with elution buffer and neutralized immediately. Immunoprecipitated proteins and input lysates were resolved by SDS-PAGE and analyzed by Western blotting using antibodies against ATF2, KAT3A/CBP/CREBBP, and NF-κB p65/RELA.

For reciprocal Co-IP, Huh-7 cell lysates were immunoprecipitated with anti-ATF2 antibody and immunoblotted for KAT3A/CBP/CREBBP and p65/RELA. Conversely, lysates were immunoprecipitated with anti-KAT3A/CBP/CREBBP or anti-p65/RELA antibody and immunoblotted for ATF2. IgG immunoprecipitation was used as a negative control, and 5% of total lysate was loaded as input.

IP-re-IP assays were performed to determine whether ATF2, KAT3A/CBP, and p65/RELA coexist in the same protein complex. Huh-7 cell lysates were first immunoprecipitated with anti-ATF2 antibody using the Pierce Crosslink Magnetic IP/Co-IP Kit. After washing, ATF2-containing immune complexes were gently eluted and immediately neutralized. The first eluate was then subjected to a second round of immunoprecipitation using anti-KAT3A/CBP/CREBBP antibody. The final immune complexes were eluted, separated by SDS-PAGE, and immunoblotted with antibodies against p65/RELA, ATF2, and KAT3A/CBP/CREBBP. Normal rabbit IgG was used as the negative control for the first and second immunoprecipitation steps. All Co-IP and IP-re-IP experiments were independently repeated three times.

Western blotting

Western blotting was performed to assess ATF2 expression, global protein lactylation, site-specific histone lactylation, and KAT3A-dependent regulation of H3K18la in HCC tissues and cells. Briefly, cultured HCC cells or freshly frozen HCC tissues were lysed in RIPA lysis buffer (Beyotime, Cat# P0013B) supplemented with protease inhibitor

cocktail (Roche, Cat# 11873580001), phosphatase inhibitor cocktail (Roche, Cat# 4906845001), 5 mM sodium butyrate (Sigma-Aldrich, Cat# B5887), and 5 mM nicotinamide (Sigma-Aldrich, Cat# N0636). Lysates were incubated on ice for 30 min and centrifuged at 12,000 × g for 15 min at 4°C. Protein concentrations were determined using the Pierce BCA Protein Assay Kit (Thermo Fisher Scientific, Cat# 23225).

For detection of histone lactylation, histones were extracted using the EpiQuik Total Histone Extraction Kit (EpiGentek, Cat# OP-0006) according to the manufacturer's instructions. Equal amounts of total protein lysates or purified histone extracts were mixed with 4× Laemmli Sample Buffer (Bio-Rad, Cat# 1610747) containing β-mercaptoethanol (Sigma-Aldrich, Cat# M3148), denatured at 95°C for 5 min, and separated by SDS-PAGE using Mini-PROTEAN TGX Precast Protein Gels (Bio-Rad, Cat# 4561084). Proteins were transferred onto Immobilon-P PVDF membranes (Millipore, Cat# IPVH00010). Membranes were blocked with 5% non-fat milk (BD Difco, Cat# 232100) in TBST for 1 h at room temperature and then incubated overnight at 4°C with the indicated primary antibodies.

The following primary antibodies were used: anti-ATF2 (Cell Signaling Technology, Cat# 35031), anti-KAT3A/CBP/CREBBP (Abcam, Cat# ab2832), anti-Pan-Kla/L-lactyllysine (PTM Bio, Cat# PTM-1401RM), anti-H3K18la (PTM Bio, Cat# PTM-1406RM), anti-H3K9la (PTM Bio, Cat# PTM-1419RM), anti-H3K14la (PTM Bio, Cat# PTM-1414RM), anti-H4K12la (PTM Bio, Cat# PTM-1411RM), anti-Histone H3 (PTM Bio, Cat# PTM-1001RM), anti-Histone H4 (PTM Bio, Cat# PTM-1015RM), anti-GAPDH (Proteintech, Cat# 60004-1-Ig), and anti-β-actin (Proteintech, Cat# 66009-1-Ig).

After washing three times with TBST, membranes were incubated with HRP-conjugated goat anti-rabbit IgG secondary antibody (Proteintech, Cat# SA00001-2) or HRP-conjugated goat anti-mouse IgG secondary antibody (Proteintech, Cat# SA00001-1) for 1 h at room temperature. Protein bands were visualized using SuperSignal West Femto Maximum Sensitivity Substrate (Thermo

Fisher Scientific, Cat# 34095) and imaged using a ChemiDoc MP Imaging System (Bio-Rad). Band intensities were quantified using ImageJ software (v1.53t). GAPDH or β-actin was used as the loading control for total cell lysates, whereas total Histone H3 or Histone H4 was used as the loading control for histone lactylation assays. Each Western blot experiment was independently repeated at least three times.

Flow cytometry

Orthotopic liver tumors were excised from mice at the indicated endpoints, minced into small fragments, and enzymatically digested in RPMI 1640 medium (Gibco, Cat# 11875093) containing collagenase IV (Worthington Biochemical, Cat# LS004188), DNase I (Roche, Cat# 10104159001), and hyaluronidase (Sigma-Aldrich, Cat# H3506) at 37°C for 30-45 min with gentle agitation. The digested tissues were passed through a 70 μm cell strainer (Falcon, Cat# 352350), washed with PBS (Gibco, Cat# 10010023), and treated with red blood cell lysis buffer (BioLegend, Cat# 420301) when necessary. Single-cell suspensions were washed and resuspended in Cell Staining Buffer (BioLegend, Cat# 420201).

For surface staining, cells were first incubated with TruStain FcX PLUS anti-mouse CD16/32 antibody (BioLegend, Cat# 156604) for 10 min at 4°C to block Fc receptors, followed by staining with Fixable Viability Stain 780 (BD Biosciences, Cat# 565388) and fluorochrome-conjugated antibodies for 30 min at 4°C in the dark.

For macrophage phenotyping, cells were stained with Brilliant Violet 510 anti-mouse CD45 (BioLegend, clone 30-F11, Cat# 103138), APC/Cyanine7 anti-mouse/human CD11b (BioLegend, clone M1/70, Cat# 101226), PE anti-mouse F4/80 (BioLegend, clone BM8, Cat# 123110), APC anti-mouse CD206/MMR (BioLegend, clone C068C2, Cat# 141708), and PerCP/Cyanine5.5 anti-mouse CD86 (BioLegend, clone GL-1, Cat# 105028). M2-like macrophages were defined as live $CD45^+CD11b^+F4/80^+CD206^+$ cells, whereas M1-like macrophages were defined as live $CD45^+CD11b^+F4/80^+CD86^+$ cells.

For T-cell exhaustion analysis, cells were stained with Brilliant Violet 510 anti-mouse CD45 (BioLegend, clone 30-F11, Cat# 103138), FITC anti-mouse CD3ε (BioLegend, clone 145-2C11, Cat# 100306), Brilliant Violet 421 anti-mouse CD8α (BioLegend, clone 53-6.7, Cat# 100738), PE/Cyanine7 anti-mouse CD279/PD-1 (BioLegend, clone 29F.1A12, Cat# 135216), and APC anti-mouse CD223/LAG-3 (BioLegend, clone C9B7W, Cat# 125210). $CD8^+$ T cells were identified as live $CD45^+CD3^+CD8\alpha^+$ cells, and T-cell exhaustion was evaluated based on PD-1 and LAG-3 expression within the $CD8^+$ T-cell population.

For intracellular cytokine staining, single-cell suspensions were stimulated for 4 h at 37°C with Cell Activation Cocktail containing PMA and ionomycin (BioLegend, Cat# 423301) in the presence of Brefeldin A Solution (BD Biosciences, Cat# 555029). After surface staining with CD45, CD3ε, and CD8α antibodies, cells were fixed and permeabilized using the Cytofix/Cytoperm Fixation/Permeabilization Kit (BD Biosciences, Cat# 554714) according to the manufacturer's instructions, followed by intracellular staining with PE anti-mouse IFN-γ (BioLegend, clone XMG1.2, Cat# 505808) and APC anti-human/mouse Granzyme B recombinant antibody (BioLegend, clone QA16A02, Cat# 372204). $CD8^+$ T-cell effector function was evaluated based on the frequency of $IFN\text{-}\gamma^+$ and $GZMB^+$ cells among live $CD45^+CD3^+CD8\alpha^+$ T cells.

Data were analyzed using FlowJo software (v10.8.1). Dead cells and doublets were excluded before downstream analysis. Fluorescence minus one controls and single-stained compensation controls were used to define gating boundaries and perform compensation. Each flow cytometry experiment was performed using biologically independent tumor samples.

RNA seq

For bulk transcriptomic analysis, we selected HCC tissue samples with high vs. low M2-macrophage infiltration status ($M2^{high}$ vs. $M2^{low}$) based on flow cytometry results. Total RNA was extracted using the RNeasy Mini Kit (Qiagen), libraries prepared via

Illumina TruSeq RNA Sample Preparation Kit, and sequencing performed on an Illumina platform. Reads were mapped to the human genome (hg38) and differential expression analysis was conducted using DESeq2; genes with $|\log_2$ fold-change$| \geqslant 1$ and adjusted $p < 0.05$ were considered differentially expressed.

Chromatin immunoprecipitation (ChIP) and ChIP-seq

Chromatin immunoprecipitation was performed using the Magna ChIP A/G Chromatin Immunoprecipitation Kit (Millipore/Sigma, Cat# 17-10085) according to the manufacturer's instructions with minor modifications. Briefly, cells were crosslinked with 1% formaldehyde (Thermo Fisher Scientific, Cat# 28906) for 10 min at room temperature, and the reaction was quenched with 125 mM glycine (Sigma-Aldrich, Cat# G8898) for 5 min. Cells were washed twice with ice-cold PBS (Gibco, Cat# 10010023), collected, and lysed in ChIP lysis buffer supplemented with protease inhibitor cocktail (Roche, Cat# 11873580001). Chromatin was fragmented to an average size of 200-500 bp by sonication using Bioruptor Pico sonication system (Diagenode).

The sheared chromatin was pre-cleared and incubated overnight at 4°C with antibodies against ATF2 (Cell Signaling Technology, Cat# 35031), NF-κB p65/RELA (Cell Signaling Technology, Cat# 6956), H3K18la (PTM Bio, Cat# PTM-1427RM), KAT3A/CBP/CREBBP (Abcam, Cat# ab2832), normal rabbit IgG (Cell Signaling Technology, Cat# 2729), or normal mouse IgG (Cell Signaling Technology, Cat# 5415). Antibody–chromatin complexes were captured using protein A/G magnetic beads. After sequential washing, chromatin was eluted, reverse-crosslinked, and treated with RNase A and proteinase K. ChIP DNA was purified using the MinElute PCR Purification Kit (Qiagen, Cat# 28004) and quantified using the Qubit dsDNA HS Assay Kit (Thermo Fisher Scientific, Cat# Q32854).

For ChIP-qPCR, purified ChIP DNA and input DNA were analyzed by quantitative PCR using TB Green Premix Ex Taq II (Takara, Cat# RR820A) on a real-time PCR

system. Primers targeting the CCL2 promoter, CCL2 enhancer, and other indicated regulatory regions were designed to amplify 80-200 bp fragments. IgG immunoprecipitation was used as the background control. For comparative analyses between control and knockdown or overexpression groups, ChIP enrichment was further normalized to the corresponding input and IgG controls. Each ChIP-qPCR experiment was performed with at least three biological replicates. Primers were listed in Supplementary Table S1.

For ChIP-seq, purified ChIP DNA was used for library preparation with the NEBNext Ultra II DNA Library Prep Kit for Illumina (NEB, Cat# E7645S/E7645L) and NEBNext Multiplex Oligos for Illumina (NEB, Cat# E7335S/E7335L). Libraries were size-selected using AMPure XP beads (Beckman Coulter, Cat# A63881), and library quality and fragment size distribution were assessed using the Agilent High Sensitivity DNA Kit (Agilent, Cat# 5067-4626). Qualified libraries were sequenced on an Illumina NovaSeq platform using paired-end sequencing.

Raw sequencing reads were quality-filtered using Trim Galore (v0.6.10) with Cutadapt (v4.4), and read quality was assessed using FastQC (v0.11.9). Clean reads were aligned to the human reference genome hg38 using Bowtie2 (v2.5.1). PCR duplicates were removed using Picard MarkDuplicates (v2.27.5), and reads with low mapping quality were filtered using SAMtools (v1.17). Peaks were called using MACS2 (v2.2.9.1) with input DNA as the background control. Genome-wide peak annotation and distribution analysis were performed using ChIPseeker (v1.36.0), motif enrichment analysis was performed using HOMER (v4.11), and ChIP-seq signal visualization, heatmap generation, and metaplot analysis were performed using deepTools (v3.5.1). Co-occupancy analyses among ATF2, p65, KAT3A, and H3K18la peaks were performed by intersecting peak regions using BEDTools (v2.30.0). Genome browser tracks were visualized using IGV (v2.16.1).

ATAC-seq

ATAC-seq was performed following the previous described[1]. Briefly, 50,000 HCC cells were harvested, washed twice with cold PBS (Gibco, Cat# 10010023), and resuspended in cold lysis buffer containing 10 mM Tris-HCl pH 7.4, 10 mM NaCl, 3 mM $MgCl_2$, 0.1% IGEPAL CA-630 (Sigma-Aldrich, Cat# I8896), 0.1% Tween-20 (Sigma-Aldrich, Cat# P9416), and 0.01% digitonin (Promega, Cat# G9441). After incubation on ice for 3 min, nuclei were collected by centrifugation at 500 × g for 10 min at 4°C and washed once with wash buffer containing 10 mM Tris-HCl pH 7.4, 10 mM NaCl, 3 mM $MgCl_2$, and 0.1% Tween-20.

The nuclear pellet was resuspended in transposition reaction mixture containing TruePrep Tagment Enzyme and TTBL buffer from the TruePrep DNA Library Prep Kit V2 for Illumina (Vazyme, Cat# TD501) and incubated at 37°C for 30 min. Transposed DNA fragments were purified using the MinElute PCR Purification Kit (Qiagen, Cat# 28004) and amplified with TruePrep Index Kit V2 for Illumina (Vazyme, Cat# TD202) and NEBNext High-Fidelity 2× PCR Master Mix (NEB, Cat# M0541S/M0541L). PCR products were purified and size-selected using AMPure XP beads (Beckman Coulter, Cat# A63881). Library concentration was measured using the Qubit dsDNA HS Assay Kit (Thermo Fisher Scientific, Cat# Q32854), and fragment size distribution was assessed using the Agilent High Sensitivity DNA Kit on an Agilent Bioanalyzer 2100 system (Agilent, Cat# 5067-4626). Qualified libraries were sequenced on an Illumina NovaSeq platform using paired-end sequencing.

Raw sequencing reads were quality-filtered using Trim Galore (v0.6.10) with Cutadapt (v4.4), and read quality was assessed using FastQC (v0.11.9). Clean reads were aligned to the human reference genome hg38 using Bowtie2 (v2.5.1). PCR duplicates were removed using Picard MarkDuplicates (v2.27.5), and reads mapped to mitochondrial DNA or ENCODE blacklist regions were excluded using SAMtools (v1.17) and BEDTools (v2.30.0). Peaks were called using MACS2 (v2.2.9.1). Differential chromatin accessibility analysis was performed using DiffBind (v3.10.0) and DESeq2 (v1.40.2). Peak annotation was performed using ChIPseeker (v1.36.0), motif enrichment analysis was conducted using HOMER (v4.11), and ATAC-seq signal

tracks, heatmaps, and metaplots were generated using deepTools (v3.5.1). Genome browser tracks were visualized using Integrative Genomics Viewer (IGV, v2.16.1).

IHC staining

Formalin-fixed, paraffin-embedded human HCC tissues, pretreatment liver biopsy specimens, and mouse tumor tissues were sectioned at 4 μm thickness and mounted on positively charged glass slides. Sections were baked at 60°C for 1 h, deparaffinized twice in xylene for 10 min each, and rehydrated through a graded ethanol series. Antigen retrieval was performed in EDTA antigen retrieval buffer, pH 9.0 (Servicebio, Cat# G1203), by heating the sections in a microwave oven at medium-high power for 8 min followed by medium-low power for 7 min. After natural cooling to room temperature, sections were washed three times with PBS.

Endogenous peroxidase activity was blocked with 3% hydrogen peroxide solution (Servicebio, Cat# G0115) for 15 min at room temperature in the dark. Sections were then blocked with 5% bovine serum albumin (BSA; Sigma-Aldrich, Cat# A7906) for 30 min at room temperature. The sections were incubated overnight at 4°C with the following primary antibodies: anti-ATF2 antibody (Cell Signaling Technology, Cat# 35031; 1:200), anti-L-lactyllysine / Pan-Kla antibody (PTM Bio, Cat# PTM-1401; 1:500), and anti-acetylated-lysine / Pan-Kac antibody (Cell Signaling Technology, Cat# 9441; 1:400).

After three washes with PBS, sections were incubated with HRP-conjugated secondary antibody using the Dako EnVision+ System-HRP kit (Agilent/Dako, Cat# K5007) for 30 min at room temperature. Immunoreactivity was visualized using DAB chromogenic substrate (Servicebio, Cat# G1212-200T), and the reaction was stopped by rinsing the slides in distilled water. Nuclei were counterstained with hematoxylin staining solution (Servicebio, Cat# G1004) for 1 min. Sections were dehydrated through graded ethanol, cleared in xylene, and mounted with neutral balsam (Solarbio, Cat# G8590).

Negative controls were processed in parallel by replacing the primary antibody with normal rabbit IgG (Cell Signaling Technology, Cat# 2729) at the same protein concentration. Images were acquired using a light microscope under identical acquisition settings. ATF2 staining was evaluated based on nuclear staining in tumor cells, whereas Pan-Kla and Pan-Kac staining were evaluated based on overall positive staining intensity in tumor regions.

IHC staining was quantified using a semi-quantitative H-score method. Staining intensity was scored as 0, negative; 1, weak; 2, moderate; and 3, strong. The percentage of tumor cells at each staining intensity was recorded, and the H-score was calculated as follows: H-score = ΣPi × i, where Pi represents the percentage of positive cells at each intensity level and i represents the staining intensity score. The final H-score ranged from 0 to 300. Staining scores were independently evaluated by two investigators blinded to clinical information and experimental grouping, and the mean value of the two scores was used for statistical analysis.

For mouse tumor tissues, ATF2 IHC staining was performed to validate ATF2 knockout or overexpression in orthotopic tumor models. H&E staining of tumor tissues and major organs was performed using an H&E staining kit (Servicebio, Cat# G1005) according to the manufacturer's protocol.

Immunofluorescence

Formalin-fixed, paraffin-embedded human HCC biopsy specimens and mouse orthotopic liver tumor tissues were cut into 4 μm-thick sections. Sections were baked at 60°C for 1 h, deparaffinized in xylene, and rehydrated through a graded ethanol series. Antigen retrieval was performed in EDTA antigen retrieval buffer, pH 9.0 (Servicebio, Cat# G1203), using microwave heating. After cooling to room temperature, sections were washed with PBS.

Sections were incubated with autofluorescence quenching reagent (Servicebio, Cat# G1221), permeabilized with 0.3% Triton X-100 (Sigma-Aldrich, Cat# T8787) for 10

min, and blocked with 5% bovine serum albumin (BSA; Sigma-Aldrich, Cat# A7906) for 30 min at room temperature.

For human HCC biopsy specimens, multiplex immunofluorescence staining was performed using primary antibodies against ATF2 (Cell Signaling Technology, Cat# 35031; rabbit monoclonal; 1:200), CD206/MRC1 (Cell Signaling Technology, Cat# 24595; rabbit monoclonal; 1:200), CD11b/ITGAM (Abcam, Cat# ab133357; rabbit monoclonal; 1:300), and CD8α (Cell Signaling Technology, Cat# 85336; rabbit monoclonal; 1:200). For mouse orthotopic liver tumor tissues, sections were stained with antibodies against CD206/MRC1 (Cell Signaling Technology, Cat# 24595; 1:200), CD11b/ITGAM (Abcam, Cat# ab133357; 1:300), and CD8α (Cell Signaling Technology, Cat# 98941; rabbit monoclonal; 1:200).

Primary antibodies were incubated overnight at 4°C. For multiplex staining, sequential staining was performed, and antibody stripping was carried out between staining cycles using citrate-based antibody stripping buffer (Servicebio, Cat# G1235) according to the manufacturer's instructions. After each primary antibody incubation, sections were incubated with species-matched Alexa Fluor-conjugated goat anti-rabbit IgG secondary antibodies, including Alexa Fluor 488 goat anti-rabbit IgG (Invitrogen, Cat# A11008; 1:500), Alexa Fluor 555 goat anti-rabbit IgG (Invitrogen, Cat# A21428; 1:500), Alexa Fluor 594 goat anti-rabbit IgG (Invitrogen, Cat# A11012; 1:500), or Alexa Fluor 647 goat anti-rabbit IgG (Invitrogen, Cat# A21245; 1:500), for 1 h at room temperature in the dark. Negative controls were processed in parallel by omitting the primary antibodies.

After completion of all staining cycles, nuclei were counterstained and sections were mounted with DAPI-containing antifade mounting medium (Abcam, Cat# ab104139). Images were acquired using a confocal laser scanning microscope under identical acquisition settings for each staining panel. ATF2 fluorescence intensity, $CD206^+$ $CD11b^+$ macrophages, and $CD8^+$ T cells were quantified in at least five randomly selected high-power fields per section using ImageJ software (v1.53t) by investigators blinded to clinical information and experimental groups.

Luciferase reporter assay

The transcriptional activity of the CCL2 promoter was evaluated using a dual-luciferase reporter assay. Human CCL2 promoter fragments, designated WT1, WT2, WT3, and WT4, were amplified from human genomic DNA and cloned into the pGL3-Basic luciferase reporter vector (Promega, Cat# E1751) using the ClonExpress II One Step Cloning Kit (Vazyme, Cat# C112). The putative ATF2-binding motif within the WT2 promoter fragment was mutated using the Q5 Site-Directed Mutagenesis Kit (New England Biolabs, Cat# E0554S) to generate the corresponding mutant reporter construct. All reporter plasmids were verified by Sanger sequencing before use. Primer sequences for promoter cloning and site-directed mutagenesis are listed in Supplementary Table S1.

For luciferase reporter assays, HCC cells were seeded into 24-well plates (Corning Costar, Cat# 3524) and cultured until they reached approximately 70-80% confluence. Cells were co-transfected with 500 ng of pGL3-Basic, pGL3-CCL2-WT1, pGL3-CCL2-WT2, pGL3-CCL2-WT3, pGL3-CCL2-WT4, or pGL3-CCL2-WT2-Mut reporter plasmid, together with 50 ng of the pRL-TK Renilla luciferase control plasmid (Promega, Cat# E2241), using Lipofectamine 3000 Transfection Reagent (Invitrogen, Cat# L3000015) according to the manufacturer's instructions. To determine the effect of ATF2 on CCL2 promoter activity, reporter constructs were transfected into control, ATF2-knockdown, ATF2-overexpressing, or corresponding vector control cells.

At 48 h after transfection, cells were washed with PBS (Gibco, Cat# 10010023) and lysed with Passive Lysis Buffer provided in the Dual-Luciferase Reporter Assay System (Promega, Cat# E1910). Firefly and Renilla luciferase activities were measured using the Dual-Luciferase Reporter Assay System on a GloMax luminometer (Promega). Firefly luciferase activity was normalized to Renilla luciferase activity to control for transfection efficiency. Relative luciferase activity was further normalized to the corresponding control group. Each experiment was performed with

three independent biological replicates, and each biological replicate included three technical replicates.

Isothermal titration calorimetry assay

Isothermal titration calorimetry (ITC) was performed to determine the binding affinity between ATF2 and histone H3 peptides. Recombinant human ATF2 protein was obtained commercially (Abnova/Novus Biologicals, Cat# H00001386-P01) and dialyzed overnight at 4°C against ITC buffer containing 20 mM HEPES (Sigma-Aldrich, Cat# H3375), 150 mM NaCl (Sigma-Aldrich, Cat# S9888), and 1 mM TCEP (Sigma-Aldrich, Cat# C4706), pH 7.5. Synthetic histone H3 peptides corresponding to residues 1-24, including the unmodified H3K18 peptide and the H3K18 lactylated peptide (H3K18la), were custom-synthesized at >95% purity by GL Biochem and dissolved in the same ITC buffer. The peptide sequences were as follows: H3K18, ARTKQTARKSTGGKAPRKQLATKA; H3K18la, ARTKQTARKSTGGKAPRKlaQLATKA, where Kla denotes lysine lactylation.

Before ITC measurement, both protein and peptide solutions were buffer-exchanged into the same ITC buffer using Amicon Ultra centrifugal filter units with a 10 kDa molecular weight cutoff (Millipore, Cat# UFC501096 or UFC901096), centrifuged at 12,000 × g for 10 min at 4°C, and degassed to remove air bubbles. ITC experiments were performed using a MicroCal PEAQ-ITC instrument (Malvern Panalytical) at 25°C. ATF2 protein was loaded into the sample cell, and histone peptide was loaded into the injection syringe. Typically, 20-30 μM ATF2 protein was titrated with 200-300 μM peptide using one initial injection of 0.4 μL followed by 18 sequential injections of 2 μL each, with a spacing time of 120-150 s between injections and a stirring speed of 750 rpm. Control titrations of peptide into ITC buffer were performed under identical conditions and subtracted from the raw binding isotherms to correct for heat of dilution.

The binding data were analyzed using MicroCal PEAQ-ITC Analysis Software

(Malvern Panalytical, version 1.41). Thermodynamic parameters, including the equilibrium dissociation constant (K_D), binding stoichiometry (N), enthalpy change (ΔH), and entropy change (ΔS), were calculated by fitting the corrected binding isotherms to a one-site binding model when applicable. Experiments were performed independently at least twice. No significant binding difference between ATF2 and unmodified H3K18 or H3K18la peptides was observed under these conditions.

GRO-seq for nascent transcription

Global run-on sequencing (GRO-seq) was performed to assess nascent transcriptional activity in HCC cells. Briefly, Huh-7 and SNU-387 cells with stable ATF2 knockdown, p65 knockdown, or the corresponding control cells were harvested and washed twice with ice-cold PBS (Gibco, Cat# 10010023). Nuclei were isolated using ice-cold nuclear isolation buffer consisting of 10 mM Tris-HCl pH 7.4 (Invitrogen, Cat# 15567027), 10 mM NaCl (Invitrogen, Cat# AM9760G), 3 mM $MgCl_2$ (Invitrogen, Cat# AM9530G), 0.1% IGEPAL CA-630 (Sigma-Aldrich, Cat# I8896), and SUPERase•In RNase Inhibitor (Invitrogen, Cat# AM2694). Isolated nuclei were immediately subjected to nuclear run-on reactions in run-on buffer containing 10 mM Tris-HCl pH 8.0, 5 mM $MgCl_2$, 300 mM KCl, 1 mM DTT, 0.5 mM ATP, 0.5 mM GTP, 0.5 mM CTP, 0.5 mM 5-bromouridine 5′-triphosphate sodium salt (BrUTP; Sigma-Aldrich, Cat# B7166), 0.5% N-lauroylsarcosine sodium salt (Sarkosyl; Sigma-Aldrich, Cat# L5125), and SUPERase•In RNase Inhibitor. The run-on reaction was performed at 30°C for 5 min to label actively transcribed nascent RNA.

Total RNA was extracted from run-on reactions using TRIzol LS Reagent (Invitrogen, Cat# 10296028) according to the manufacturer's instructions. Genomic DNA was removed by treatment with TURBO DNase (Invitrogen, Cat# AM2238). BrUTP-labeled nascent RNA was enriched using anti-BrdU agarose beads (Santa Cruz Biotechnology, Cat# sc-32323 AC). After stringent washing, BrU-labeled RNA was eluted, purified using the RNA Clean & Concentrator-5 Kit (Zymo Research, Cat#

R1013), and quantified using the Qubit RNA HS Assay Kit (Thermo Fisher Scientific, Cat# Q32852).

Purified nascent RNA was used for strand-specific library construction with the NEBNext Multiplex Small RNA Library Prep Set for Illumina (NEB, Cat# E7300S) according to the manufacturer's instructions. Libraries were purified using AMPure XP beads (Beckman Coulter, Cat# A63881). Library quality and fragment size distribution were assessed using the Agilent High Sensitivity DNA Kit on an Agilent Bioanalyzer 2100 system (Agilent, Cat# 5067-4626). Qualified libraries were sequenced on an Illumina NovaSeq 6000 platform using paired-end 150 bp sequencing.

Raw sequencing reads were quality-filtered using Trim Galore (v0.6.10) with Cutadapt (v4.4), and read quality was assessed using FastQC (v0.11.9). Clean reads were aligned to the human reference genome hg38 using Bowtie2 (v2.5.1). PCR duplicates were removed using Picard MarkDuplicates (v2.27.5), and low-quality reads were filtered using SAMtools (v1.17). Strand-specific GRO-seq signal tracks were generated using deepTools (v3.5.1). Sense and antisense nascent transcription at target loci, including CCL2, IL-6, and CD54/ICAM1, was visualized using Integrative Genomics Viewer (IGV, v2.16.1). Differential nascent transcription analysis between control and knockdown groups was performed using DESeq2 (v1.40.2).

For locus-specific validation, BrUTP-labeled nascent RNA was reverse-transcribed using the PrimeScript RT reagent Kit with gDNA Eraser (Takara, Cat# RR047A), and nascent RNA levels of CCL2, IL-6, and CD54/ICAM1 were quantified by RT-qPCR using TB Green Premix Ex Taq II (Takara, Cat# RR820A). Enhancer RNA levels at the CCL2 regulatory region were also quantified by RT-qPCR using primers targeting ATAC-seq-defined and H3K18la/p65-enriched enhancer regions. Relative nascent RNA and eRNA levels were calculated using the $2^{-\Delta\Delta Ct}$ method. Each experiment was performed with three biological replicates. Primers were listed in Supplementary Table S1.

ELISA

Secreted CCL2 levels in HCC cell culture supernatants were measured using a human CCL2/MCP-1 ELISA kit. Briefly, HCC cells with ATF2 knockdown, ATF2 overexpression, CCL2 knockdown, CCL2 restoration, and the corresponding control cells were seeded into 6-well plates at equal density and cultured until they reached approximately 70–80% confluence. Cells were washed twice with sterile PBS and then cultured in serum-free medium for 48 h. Culture supernatants were collected and centrifuged at 1,000 × g for 10 min at 4°C to remove cell debris. The clarified supernatants were stored at −80°C until analysis.

CCL2 concentrations were determined using the Human CCL2/MCP-1 Quantikine ELISA Kit (R&D Systems, Cat# DCP00) according to the manufacturer's instructions. Standards and samples were added to the pre-coated microplate and incubated for 2 h at room temperature. After washing, human CCL2 conjugate was added and incubated for 1 h at room temperature. The plate was washed again, followed by incubation with substrate solution for 30 min in the dark. The reaction was terminated using stop solution, and absorbance was measured at 450 nm with wavelength correction at 570 nm using a microplate reader. CCL2 concentrations were calculated from the standard curve and normalized to the total cell number of each well. Each sample was measured in technical duplicate, and each experiment was performed with three biological replicates.

References

1. Grandi, F.C., et al., *Chromatin accessibility profiling by ATAC-seq.* Nature Protocols, 2022. **17**(6): p. 1518-1552.

Supplementary figures and figure legends

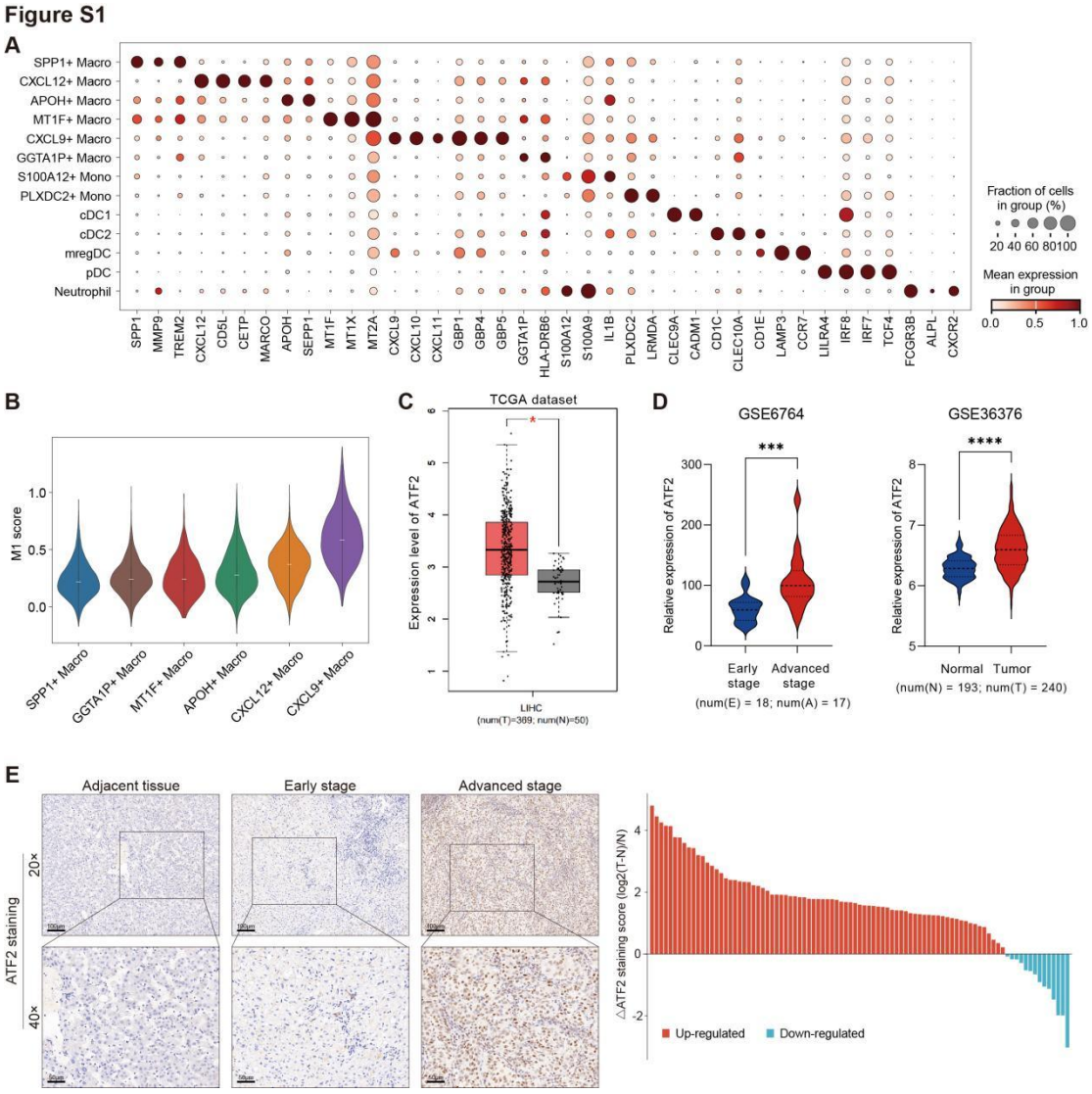

Figure S1. Expression pattern of ATF2 in HCC and its association with macrophage subpopulations, related to Figure 1. (A) Bubble plot showing average expression of marker genes to identify different clusters in myeloid subtype. **(B)** Violin plots depicting the M1 polarization scores of representative macrophage subsets (SPP1^{+}, GSTATP1^{+} , MT1F^{+} , APOH^{+} , CXCL12^{+} , and CXCL9^{+} macrophages) in the single-cell dataset. **(C)** Box plot showing ATF2 expression levels in HCC and adjacent normal liver tissues from the TCGA-LIHC dataset (n = 396 tumor, n = 50 normal). **(D)** Violin plots illustrating the relative ATF2 mRNA expression in early-stage and advanced-stage HCC samples (GSE6764) and in normal versus tumor tissues (GSE36376). **(E)** Representative immunohistochemical (IHC) staining images of ATF2

in adjacent, early-stage, and advanced-stage HCC tissues with quantitative comparison of ATF2 staining scores across paired samples. Data are shown as mean ± SEM. Statistical significance was determined by two-tailed Student's t-test for two-group comparisons and one-way ANOVA followed by Tukey's multiple-comparisons test for comparisons among multiple groups (*P < 0.05, **P < 0.01, ***P < 0.001).

Figure S2

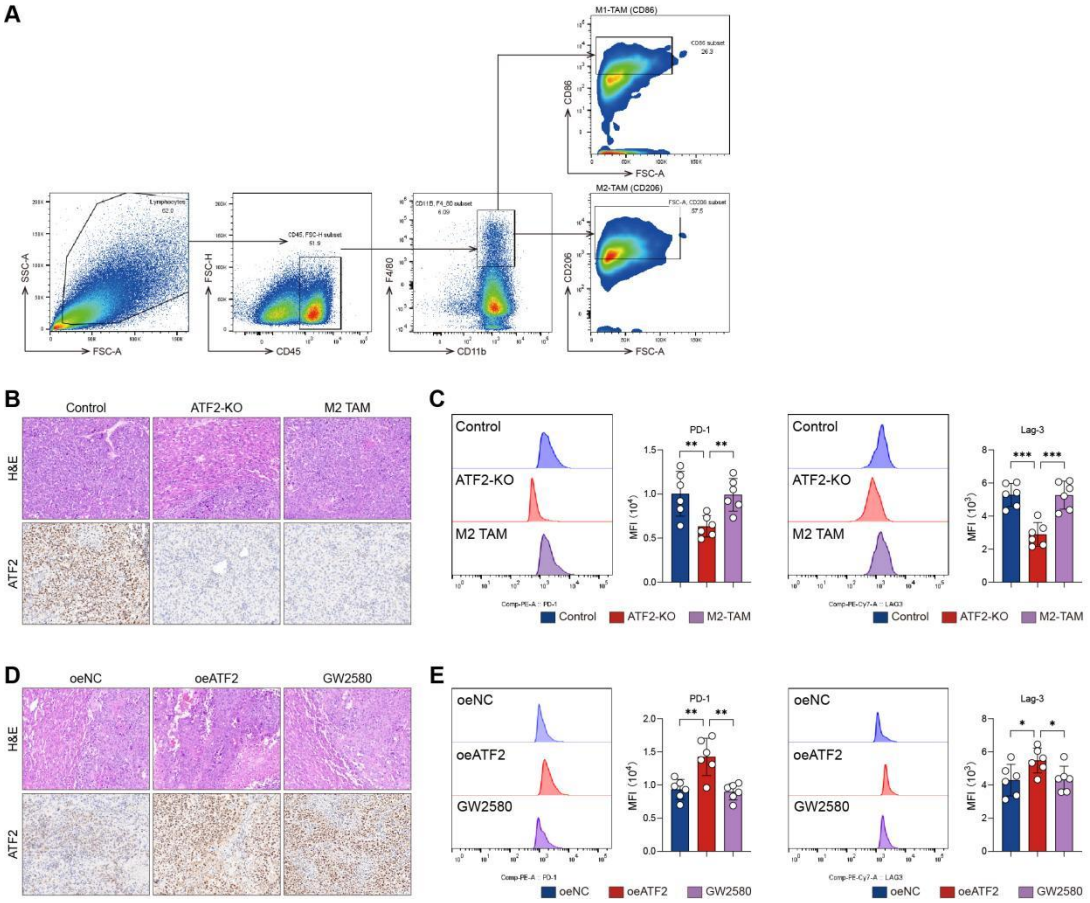

Figure S2. ATF2 promotes M2-like polarization and induces immunosuppressive TME in HCC, related to Figure 2. (A) Gating strategy for macrophage polarization by flow cytometry. **(B)** Representative images of H&E (upper panel) and IHC for ATF2 in mice liver tumors from each group (n = 6). **(C)** Flow cytometry results showing T cell exhausted markers PD-1 and Lag-3 expression levels in each group (n = 6). **(D)** Representative images of H&E (upper panel) and IHC

for ATF2 in mice liver tumors from each group (n = 6). **(E)** Flow cytometry results showing T cell exhausted markers PD-1 and Lag-3 expression levels in each group (n = 6). Data are shown as mean ± SEM; Statistical significance was determined by two-tailed Student's t-test for two-group comparisons and one-way ANOVA followed by Tukey's multiple-comparisons test for comparisons among multiple groups (*P < 0.05, **P < 0.01, ***P < 0.001).

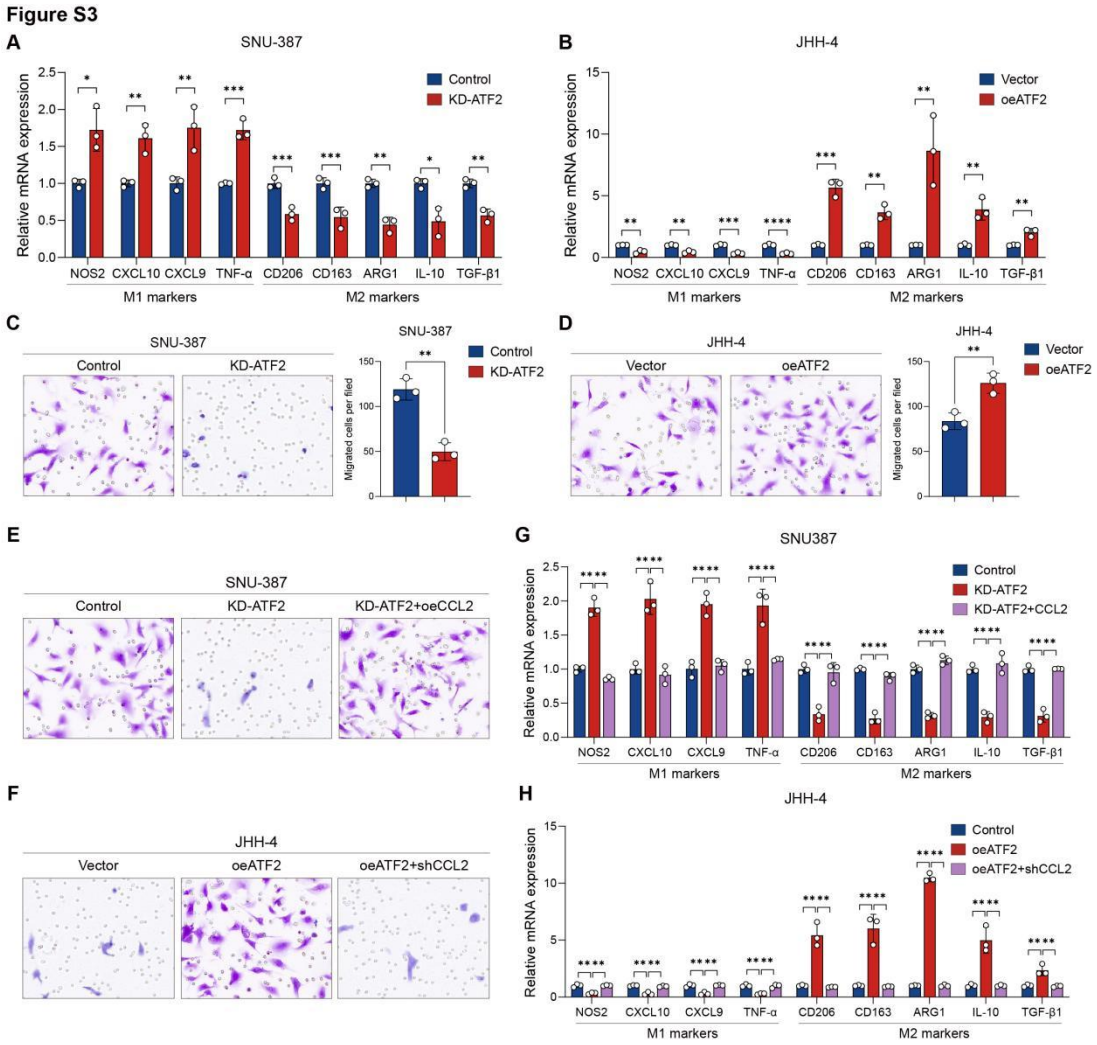

Figure S3. The intrinsic activity of ATF2 in tumor cells drives macrophage M2-type polarization and recruitment by modulating CCL2 expression, related to Figure 3. (A) RT-qPCR analysis showing the indicated M1-associated genes (NOS2, CXCL10, CXCL9, TNF-α) and M2-associated genes (CD206, CD163, ARG1, TGF-β1, IL-10) expression levels in ATF2 knockdown HCC cells. **(B)** RT-qPCR

analysis showing the indicated M1-associated genes (NOS2, CXCL10, CXCL9, TNF-α) and M2-associated genes (CD206, CD163, ARG1, TGF-β1, IL-10) expression levels in ATF2 overexpressing HCC cells. **(C-D)** Chemotaxis assays showing the effect of supernatants from the indicated co-culture system on the migration ability of macrophage-differential THP-1 cells. **(E-F)** Chemotaxis assays showing the effect of supernatants from the indicated co-culture system on the migration ability of macrophage-differential THP-1 cells to confirm CCL2 is the key downstream mediator for ATF2. **(G-H)** RT-qPCR analysis showing the indicated M1-associated genes (NOS2, CXCL10, CXCL9, TNF-α) and M2-associated genes (CD206, CD163, ARG1, TGF-β1, IL-10) expression levels in HCC cells with ATF2 or CCL2 modulations. Data are shown as mean ± SEM. Statistical significance was determined by two-tailed Student's t-test for two-group comparisons and one-way ANOVA followed by Tukey's multiple-comparisons test for comparisons among multiple groups (*P < 0.05, **P < 0.01, ***P < 0.001).

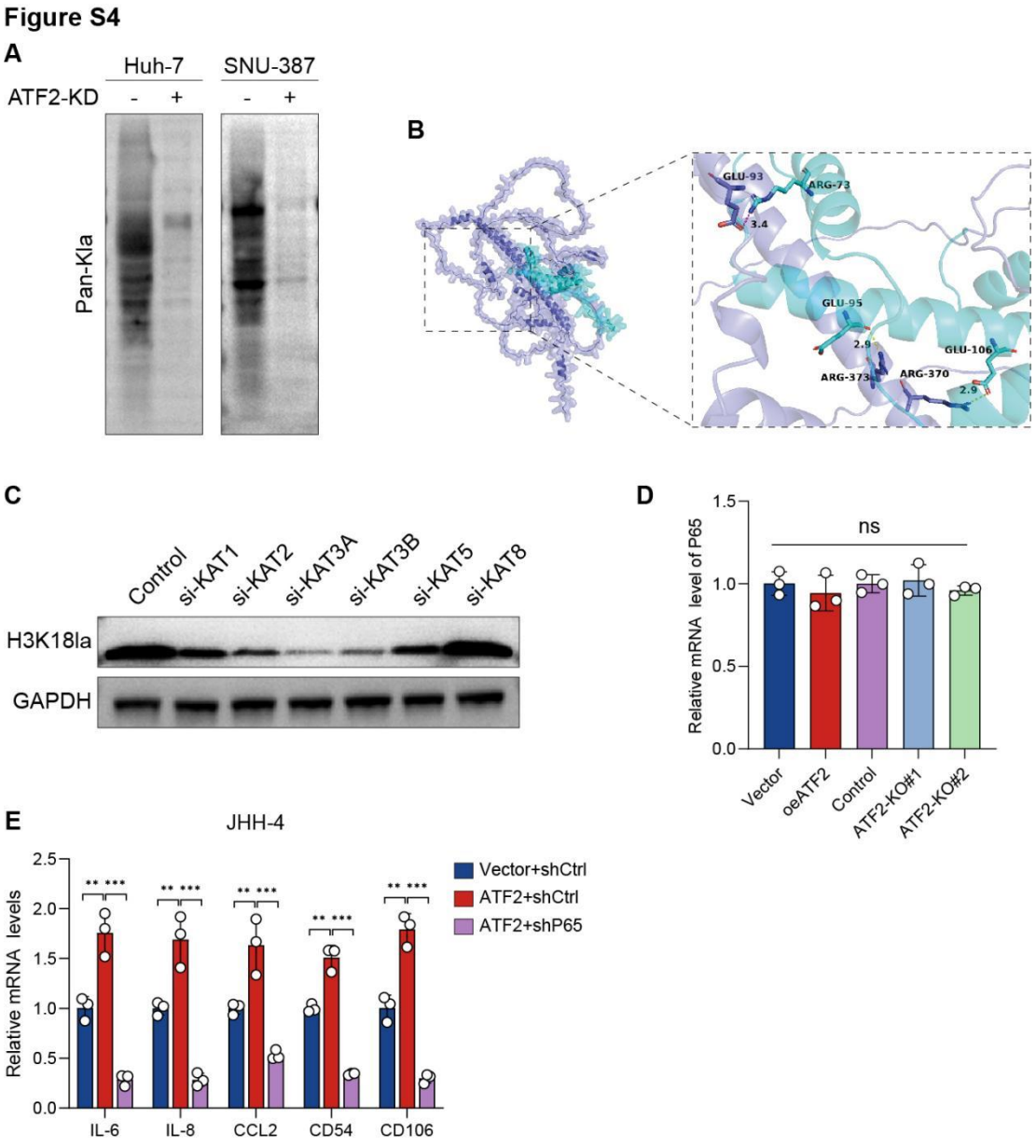

Figure S4. ATF2 cooperates with KAT3A to promote histone lactylation, particularly H3K18la, without direct binding to lactylated histones, related to Figure 4 and 5. (A) Western blot analysis showing a significant reduction in overall protein lactylation levels in ATF2-knockdown HCC cells compared with control cells. **(B)** Molecular docking simulations predicting the interaction between ATF2 and H3K18la peptides, indicating no stable physical docking interface between the two proteins. **(C)** Western blot analysis of H3K18la levels following knockdown of the indicated histone lactylation “writer” enzymes. **(D)** RT-qPCR result showed the mRNA levels of p65 after knockdown or overexpression of ATF2. **(E)** RT-qPCR validation

confirming selective downregulation of NF-κB target genes in JHH-4. Data are shown as mean ± SEM; Statistical significance was determined by two-tailed Student's t-test for two-group comparisons and one-way ANOVA followed by Tukey's multiple-comparisons test for comparisons among multiple groups (*P < 0.05, **P < 0.01, ***P < 0.001).

Figure S5

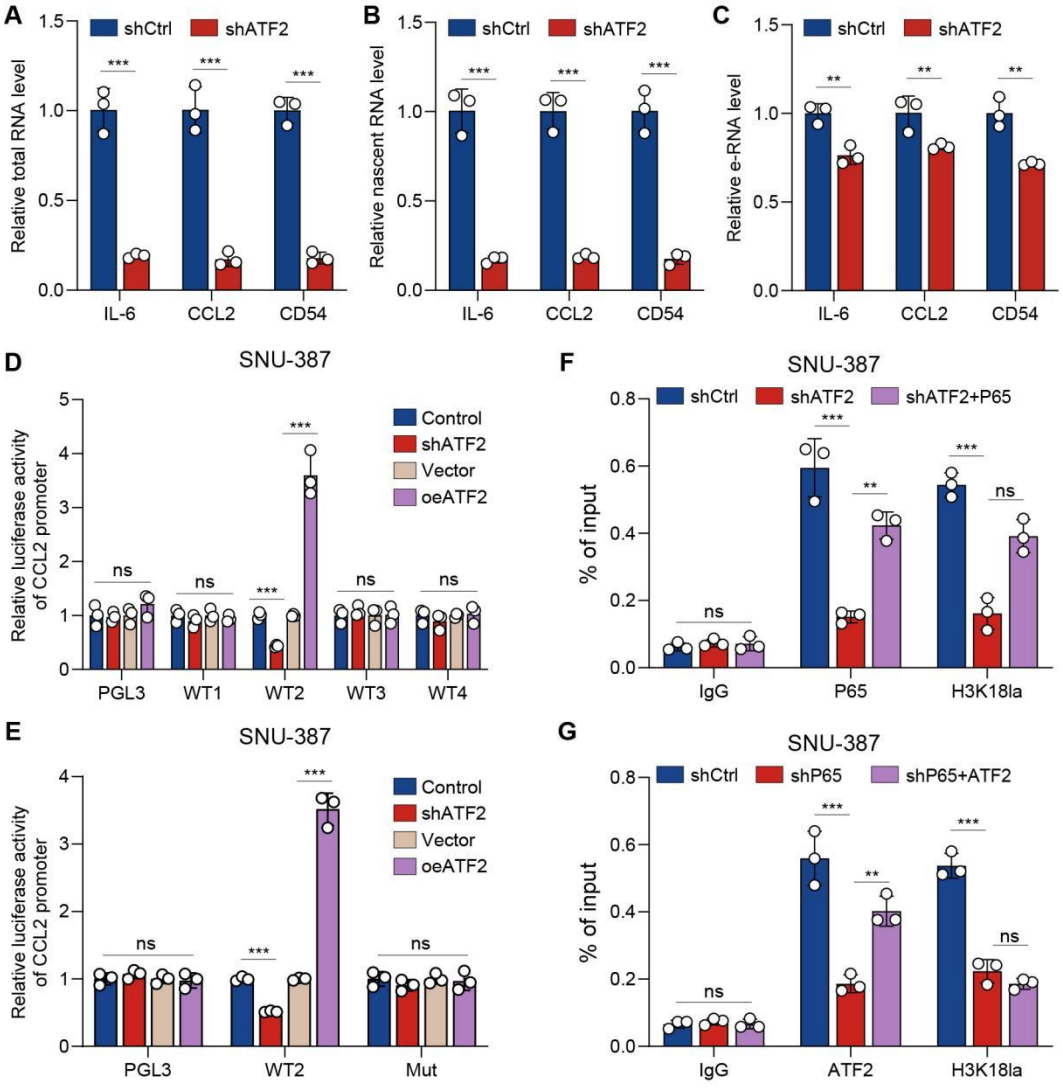

Figure S5. ATF2 directly activates the CCL2 promoter and facilitates p65 recruitment through H3K18la modification, related to Figure 6. (A-C) RT-qPCR analysis showing the relative total RNA **(A)**, nascent RNA **(B)**, and enhancer RNA (eRNA) **(C)** levels of IL-6, CD54, and CCL2 following p65 knockdown in Huh-7 cells.

(D) Dual-luciferase reporter assays of SNU-387 cells transfected with wild-type (WT1-WT4) or control (PGL3) CCL2 promoter constructs, combined with ATF2 knockdown or overexpression. **(E)** Mutational analysis of the ATF2-binding motif within the WT2 promoter region in SNU-387 cells. **(F-G)** ChIP-qPCR analyses demonstrating that ATF2 knockdown significantly reduced p65 binding and H3K18la enrichment at the CCL2 promoter **(F)**, while p65 depletion did not affect ATF2 occupancy but decreased H3K18la levels **(G)**. Data are shown as mean ± SEM; Statistical significance was determined by two-tailed Student's t-test for two-group comparisons and one-way ANOVA followed by Tukey's multiple-comparisons test for comparisons among multiple groups (*P < 0.05, **P < 0.01, ***P < 0.001).

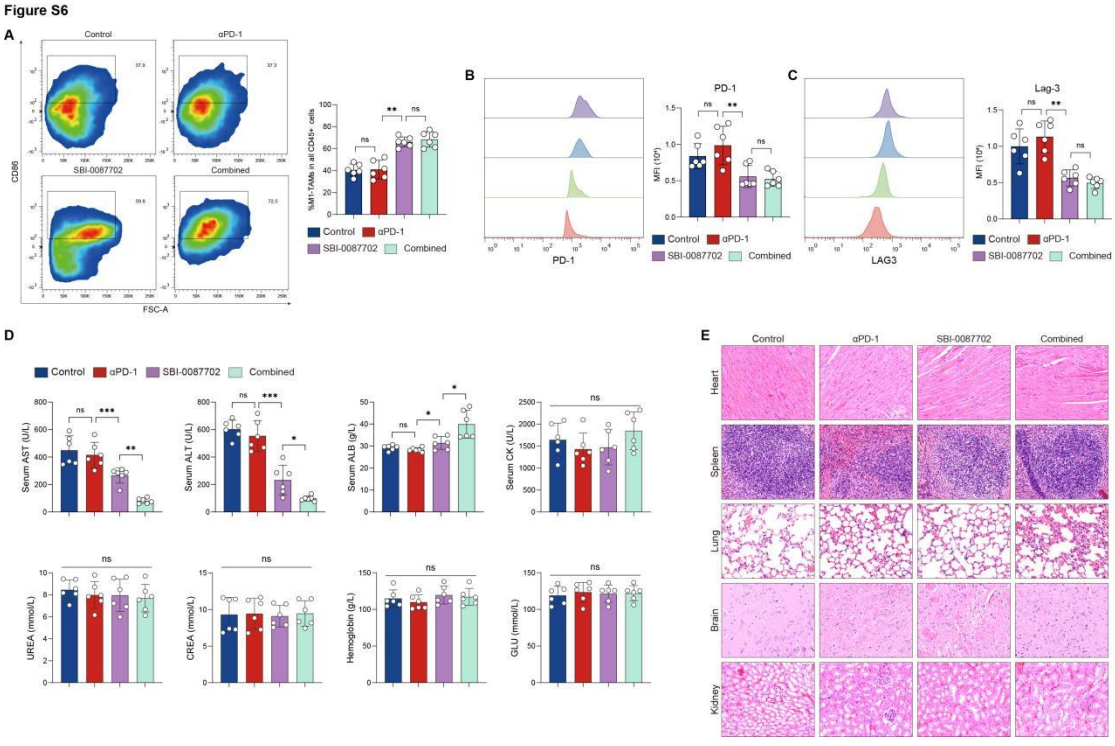

Figure S6. Safety evaluation and immune profiling following ATF2 inhibition combined with αPD-1 therapy in orthotopic HCC models, related to Figure 7. (A) Flow cytometric analysis of tumor-infiltrating macrophages showing the proportion of $CD86^+$ (M1-like) populations among $CD45^+$ immune cells. **(B-C)** Flow cytometric histograms and quantification of PD-1 **(B)** and LAG-3 **(C)** expression on intratumoral $CD8^+$ T cells. **(D)** Serum biochemical parameters in treated mice, including AST, ALT,

ALB, CK, UREA, CREA, hemoglobin (HGB), and glucose (GLU). **(E)** Representative hematoxylin and eosin (H&E) staining of major organs (heart, spleen, lung, brain, and kidney) from each treatment group. Data are shown as mean ± SEM; Data are shown as mean ± SEM. Statistical significance was determined by two-tailed Student's t-test for two-group comparisons and one-way ANOVA followed by Tukey's multiple-comparisons test for comparisons among multiple groups (*P < 0.05, **P < 0.01, ***P < 0.001).